A Hierarchical Segmentation of Articulated Bodies

Fernando de Goes[1], Siome Goldenstein[1], and Luiz Velho[2]

[1]Instituto de Computação - Universidade Estadual de Campinas - Campinas, SP, Brazil
[2]IMPA - Instituto de Matemática Pura e Aplicada - Rio de Janeiro, RJ, Brazil

Abstract
This paper presents a novel segmentation method to assist the rigging of articulated bodies. The method computes a coarse-to-fine hierarchy of segments ordered by the level of detail. The results are invariant to deformations, and numerically robust to noise, irregular tessellations, and topological short-circuits. The segmentation is based on two key ideas. First, it exploits the multiscale properties of the diffusion distance on surfaces, and then it introduces a new definition of medial structures, composing a bijection between medial structures and segments. Our method computes this bijection through a simple and fast iterative approach, and applies it to triangulated meshes.

Categories and Subject Descriptors (according to ACM CCS): I.3.5 [Computer Graphics]: Computational Geometry and Object Modeling

1. Introduction

Character articulation is a fundamental and time consuming task in animation systems. The rigging of a 3D character can be effectively oriented by segmentation methods. This appeals to the fact that the segmentation identifies joints and meaningful regions. Furthermore, the segmentation can also provide different levels of details. In the coarser levels, the segments indicate functional regions, such as arms and legs. In the finer levels, the segments correspond to rigid components, approximating the bones of a skeleton.

In this paper, we present a novel method to segment articulated bodies. Our approach recovers the articulation structure of the model, resulting in a coarse-to-fine hierarchy of segments. The method is based on two main concepts. First, we investigate a family of metrics called *diffusion distance* [CL06]. The diffusion distance defines a multi-scale metric with nice properties, such as robustness to noise and topologic events, enhancement of concave regions, and invariance to isometric deformations. Second, we introduce a generalization of the *medial structures* [MPS*04]. At each level of detail, we decompose the model computing a bijection between the medial structures and the segments.

1.1. Related Work

Mesh segmentation has become a commonplace in many graphics applications, ranging from simplification, parameterization, and shape matching. For surveys, see [Sha04,

AKM*06, Sha06]. Here, we focus on the problem of segmenting articulated bodies into meaningful regions.

Many segmentation methods are based on cognition studies. Cognition researches [HR84, HS97] have shown that the human vision breaks a shape in salient parts, setting the boundaries in concave regions. To reproduce the cognition studies, some methods incorporate concavity measures into clustering techniques [MW99, STK02, PKA03, LZ04]. In particular, Katz and Tal [KT03] extracted skeletons using a fuzzy clustering with graph cuts and a metric that combines geodesic distances and dihedral angles. Lee et al. [LLS*05] also exploited cognition studies and presented a semi-automatic detection of salient contours in 3D models. Their method applies geometric-snakes over the points with minimum curvature values.

Local attributes, such as dihedral angles and curvatures, are sensitive to noise and to mesh resolution. As a consequence, the previous methods suffer from numerical instability. In our approach, we use the diffusion distance to achieve the cognition results with numerical robustness. By construction, the diffusion distance emphasizes the concavities of a model, measuring the rate of Brownian paths between points (Sec. 2.1). This averaging scheme also reduces the interference of noise and sampling.

Some segmentation methods identify meaningful regions through the detection of geometric features. Hilaga et

al. [HSKK01] defined a feature point as a local maximum of the *A*verage *G*eodesic *D*istance function (*AGD*). Geometrically, the *AGD* measures how isolated a surface point is. In [KLT05], the *AGD* features were used as anchor points of a spherical mirroring to extract the core component of 3D models. In [ZMT05], the segments were decomposed through the analysis of the area variation around the *AGD* features. Zhang and Liu [ZL05, LZ07] computed meaningful segments recursively, using a linear search with salient cut metrics from each extracted feature point. In [ZL05], the feature points were estimated approximating the *AGD* by a small set of reference faces. In [LZ07], the feature selection was improved via spectral embedding and contour analysis.

Despite the fact that feature points identify segments, a segment may not have a feature point. Therefore, feature-based methods may fail, and thus create an incomplete hierarchy of details. We avoid these problems introducing a new structure to identify the segments at each level of detail. Our structure is a generalization of the medial structures proposed by [MPS*04]. Originally, the medial structures were computed as loops in tubular regions. Here, we define a medial structure as the set of points with the smallest average of the diffusion distance (Sec 2.2).

Recent techniques approximate meaningful segments by convex components. In [LKA06], an iterative approach generated hierarchical segmentations and multi-resolution skeletons using the approximate convex decomposition method [LA04]. Kreavoy et al. [KJS07] used segmentation to create a model composition system from interchangeable components. The models were decomposed into a hierarchy of nearly convex components using a variational decomposition method [KS06]. Because the convex segments approximate rigid components, the hierarchy of segments is built in a bottom-up fashion. This requires the computation of finer segmentations and also a merging step. In our approach, we compute a coarse-to-fine hierarchy of details.

Example-based approaches [MG03,AKP*04,JT05,SY07] learn skeletons and skinning weights from a set of reference poses. These methods decompose the poses simultaneously, and guarantee results consistent to deformations. Our algorithm computes consistent segments from a single pose of the model. We achieve consistency because the diffusion distance is invariant to isometric deformations. In [Rus07], a variation of the diffusion distance was introduced as an invariant shape descriptor and, combined with k-means clustering, it also generated consistent segments. While this descriptor embeds the surface in an unique level of detail, we exploit the scale space offered by the diffusion distance.

At last, Shapira et al. [SSCO08] presented a segmentation algorithm based on the *S*hape *D*iameter *F*unction (*SDF*). The *SDF* links local shape volumes to the surface by measuring a shape-diameter. The *SDF* is oblivious to any deformation that does not alter the volumetric shape locally, and, therefore, it is appropriated for consistent segmentation. The segments are computed using a Gaussian mixture model to cluster the histogram of *SDF* values. The number of Gaussian indicates the level of the segmentation hierarchy, and not the number of segments. Consequently, the segments at one level are independent from previous levels, and may not compose a hierarchical tree.

1.2. Contributions

The main contributions of our work are:

- We present a novel segmentation method for articulated bodies. Our results are robust to noise and mesh tessellation, and consistent to isometric deformations.
- We review the diffusion distance on surfaces, and discuss its benefits for the segmentation problem.
- We introduce a new definition of medial structures, and formulate a bijection between them and the segments.
- We describe a simple iterative algorithm to compute the bijection between segments and medial structures, recovering the hierarchy of segments of articulated bodies.

2. Theory

In the following, we present the two essential concepts for our segmentation method. First, we review the family of diffusion distances, and discuss some relevant properties. After, we introduce the definition of medial structures, and describe the bijection between segments and medial structures.

2.1. Diffusion Distance

Diffusion distance was first presented for stochastic dynamic systems, and applied to the problem of dimensionality reduction and data parameterization [CL06]. In this context, given a Markov Random Field defined on a data set $\mathcal{X}$, the diffusion distance between two points x and y at a time step t is given by:

$$\mathcal{D}_t^2(x,y) = \int_{\mathcal{X}} (p_t(x,z) - p_t(y,z))^2 d\mu(z), \qquad (1)$$

where $p_t(\cdot,\cdot)$ is the probability to walk between two points in less than or equal to t steps, and $\mu(\cdot)$ is the distribution of points in $\mathcal{X}$.

The diffusion distance indicates the rate of connectivity between the points of $\mathcal{X}$. This measure will be small if there are a lot of random walks of time less than or equal to t, and it will be large if, on the contrary, the number of random walks is small.

In this work, we restrict the data set to compact and continuous two-dimensional manifold $\mathcal{M}$ (boundaries are allowed). It is well-known in stochastic processes (c.f. [Bas95]) that, in the scaling limit, random walks on $\mathcal{M}$ are equivalent to Brownian paths, and the probability function $p_t(\cdot,\cdot)$ converges to the heat kernel $\mathcal{K}_t(\cdot,\cdot)$ of $\mathcal{M}$. In this sense, the diffusion distance between points of $\mathcal{M}$ measures the rate of Brownian paths at the time scale t,

$$\mathcal{D}_t^2(x,y) = \int_{\mathcal{M}} (\mathcal{K}_t(x,z) - \mathcal{K}_t(y,z))^2 dz. \qquad (2)$$
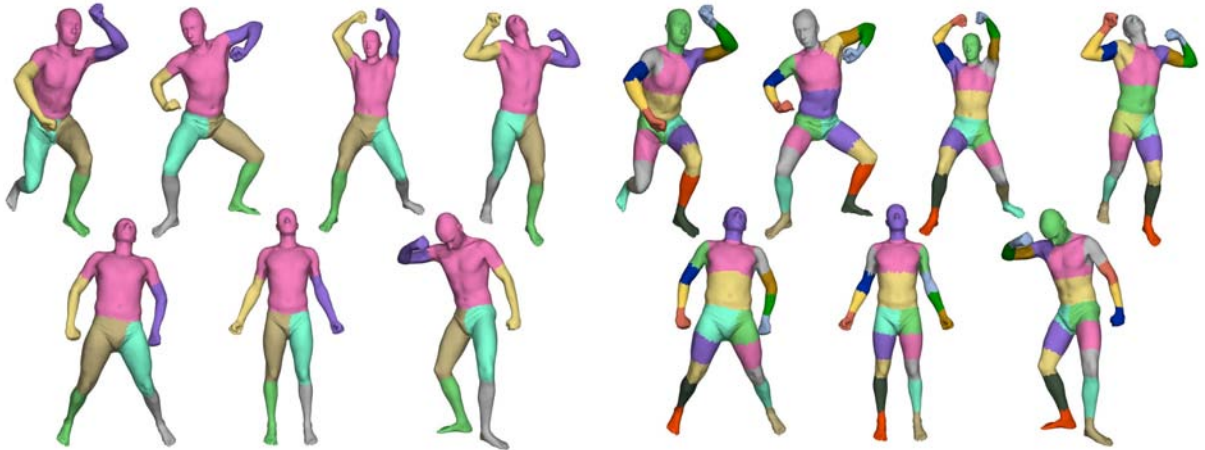
Figure 1: *Consistent segmentations in successive scales of seven poses of a scanned human model [AKP*04]. The images show the segments of the first and second levels of details, respectively.*

The averaging scheme introduced by the diffusion distance provides desirable properties for the segmentation problem. First of all, it makes the measures robust to noise and to topological short-circuits. Unlike geodesic distances, the diffusion distance increases greatly through shrunken regions, and then highlights concavities of $\mathcal{M}$ (Fig. 3).

Another advantage of the diffusion distance is the multi-scale analysis provided by the time parameter t, expanding the diffusion distance to a family of metrics. In long time intervals, the diffusion distance evaluates global structures of $\mathcal{M}$, and in shorter time intervals, the measures become local and sensitive to small features.

The heat kernel $\mathcal{K}_t(\cdot,\cdot)$ is determined by the eigenvalues and eigenfunctions of the laplacian operator,

$$\mathcal{K}_t(x,y) = \sum_{k=0}^{\infty} e^{-\lambda_k t} \phi^k(x) \phi^k(y). \quad (3)$$

In surfaces (or higher dimension manifolds), the laplacian is generalized by the Laplace-Beltrami operator. Its eigenvalues compose an increasing sequence $0 = \lambda_0 < \lambda_1 \leq \ldots \uparrow \infty$, and its eigenfunctions ϕ^k are functions on $\mathcal{M}$ with increasing oscillations. Each pair (λ_k, ϕ^k) corresponds to a solution of the stationary Helmholtz equation,

$$\Delta \phi^k = -\lambda_k \phi^k. \quad (4)$$

The Laplace-Beltrami operator is invariant to isometries. This means that, if $\mathcal{M}$ is deformed preserving the geodesic distances, the Laplace-Beltrami operator will not change. As a consequence, the pairs (λ_k, ϕ^k), the heat kernel, and the family of diffusion distances are also invariant to isometries. This property enables our method to segment different poses of an object in a consistent way.

Following [CL06], we can replace Eq. 3 into Eq. 2, and

rewrite the diffusion distance in term of *diffusion maps*,

$$\Phi_t(x) = \left(\cdots e^{-\lambda_k t} \phi^k(x) \cdots \right)^T. \quad (5)$$

Then, the diffusion distance becomes an euclidian distance between vectors of infinity dimension,

$$\mathcal{D}_t^2(x,y) = \|\Phi_t(x) - \Phi_t(y)\|^2 = \sum_{k=1}^{\infty} e^{-2\lambda_k t} (\phi^k(x) - \phi^k(y))^2. \quad (6)$$

Since the eigenvalues $\{\lambda_k\}$ increase rapidly, we can truncate the diffusion maps and approximate the diffusion distance using just the first terms of the sum. Henceforth, we refer to $\Phi_t(\cdot)$ as the vector with $e^{-\lambda_k t} > \delta$, where $\delta = 0.1$.

2.2. Medial Structure

Now, we discuss how to identify the meaningful components of a region $\mathcal{R} \subset \mathcal{M}$. We address this issue using the diffusion distance to formulate a bijection between the medial structures and the segments of $\mathcal{R}$. In one way of the bijection, we compute the medial structures from the segments of $\mathcal{R}$. In the opposite way, we compute the segments from the medial structures.

In the remaining, we refer $t_{\mathcal{R}}$ as the time scale of the diffusion distance sufficient to emphasize the global concavities of $\mathcal{R}$, filtering its small features.

Segments → Medial Structures

Given a segment $\mathcal{R}_i \subset \mathcal{R}$, we characterize $\mathcal{R}_i$ by its medial structure. In [MPS*04], medial structures were introduced as loops equidistant to the boundaries of tubular regions. Here, we set a medial structure as the most distant points from the concavities of the segment. Note that medial structures differ from medial axis, since the former is medial with respect to the segments.

To compute the medial structure of $\mathcal{R}_i$, we evaluate the *Average Diffusion Distance* function (*ADD*):

$$ADD(x) = \frac{1}{A_{\mathcal{R}_i}} \int_{\mathcal{R}_i} \mathcal{D}_{t_{\mathcal{R}}}^2(x,y)dy. \qquad (7)$$

Similar to the *AGD* [HSKK01], the *ADD* presents high values for boundary and extrema points, and small values for points in the center of the segment. Because the *ADD* inherits the properties of the diffusion distance, the points with small *ADD* values correspond to distant points from the concavities (Fig. 2(a)). Therefore, we define the medial structure $\mathcal{S}_i$ of the segment $\mathcal{R}_i$ as:

$$\mathcal{S}_i = \left\{ x \in \mathcal{R}_i : ADD(x) = \min_{y \in \mathcal{R}_i} ADD(y) \right\}. \qquad (8)$$
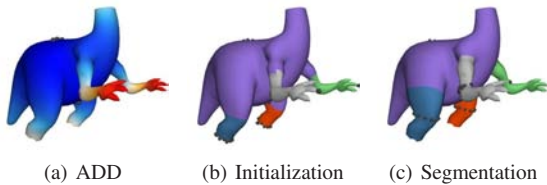
Medial Structures → Segments
Given the medial structures $\{\mathcal{S}_i\}$ of $\mathcal{R}$, we employ competing fronts to recover the segments $\{\mathcal{R}_i\}$. Each front $\mathcal{F}_i$ is propagated by increasing the iso-value d of the diffusion distance relative to $\mathcal{S}_i$,

$$\mathcal{F}_i(d) = \left\{ x \in \mathcal{R} : \min_{y \in \mathcal{S}_i} \mathcal{D}_{t_{\mathcal{R}}}^2(x,y) = d \right\}. \qquad (9)$$

The competition starts from the medial structures, $\mathcal{F}_i(0)$, and ends when all the fronts collapse.

During propagation, we set each segment $\mathcal{R}_i$ as the region covered by the respective front $\mathcal{F}_i$. Since the concavities at $t_{\mathcal{R}}$ are distant from the medial structures, the boundaries of segments tend to reside in the concavities. Fig. 3 shows with colors the front propagation from different medial structures. Observe that the iso-values d increase rapidly in the meaningful concavities of the model.

3. Algorithm

    (a) ADD   (b) Initialization   (c) Segmentation
Figure 2: *Spheres represent the points of the medial structures. (a) The ADD function of the region and its medial structure. The colors indicate the ADD values, increasing from blue to red. (b) The initial medial structures and segments. (c) The final segmentation with the bijection between the segments and the medial structures.*

Based on the concepts of Sec. 2, we present our algorithm for the segmentation problem. Here, we describe it for triangulated meshes $\mathcal{M} = (V, E, F)$, but it can be easily extended to different surface representations (e.g., point clouds).

In a triangulated mesh $\mathcal{M} = (V, E, F)$, we discretize a function f by the vector $\vec{f}$, where f_i is the value of f on the vertex $i \in V$. For points inside the triangles, we approximate f using linear interpolation and barycentric coordinates.

Figure 3: *Front propagation from each medial structure. Spheres indicate the points of the medial structures. Colors encode the iso-values of the diffusion distance between the medial structures and the surface points, ranging from blue to red. Note that the colors change greatly in the concavities.*

As a pre-processing stage, we compute the eigen-pairs $(\lambda_k, \vec{\phi}^k)$ of the Laplace-Beltrami operator of $\mathcal{M}$ (Eq. 4). In our implementation, we use the solver proposed in [VL08], which handles meshes with up a million of vertices and irregular tessellations with computational time linear in the number of eigen-pairs.

Given a region $\mathcal{R} \subset \mathcal{M}$, first we select a time scale $t_{\mathcal{R}}$. We exploit the fact that larger area may contain more global structures, and set

$$t_{\mathcal{R}} = \frac{1}{2\lambda_1} \frac{A_{\mathcal{R}}}{A_{\mathcal{M}}}, \qquad (10)$$

where $A_{\mathcal{R}}$, $A_{\mathcal{M}}$ are the areas of $\mathcal{R}$, $\mathcal{M}$, respectively. The constant $1/2\lambda_1$ makes the time selection invariant to the scale of $\mathcal{M}$ (see [RWP06]). Then, we compute the diffusion maps $\Phi_{t_{\mathcal{R}}}$ for all the vertices of $\mathcal{R}$.

We decompose a region $\mathcal{R}$ by computing the bijection between its medial structures and segments. For that matter, our algorithm has an initialization step and a main loop.

During initialization, we compute the number of segments in $\mathcal{R}$, and an initial guess for the medial structures $\{\mathcal{S}_i\}$ (Fig. 2(b)). We start setting the medial structure of $\mathcal{R}$, $\mathcal{S}_{\mathcal{R}}$, as the first medial structure, $\mathcal{S}_1$. Then, recursively, we select the most distant vertex $v \in \mathcal{R}$ from the previous medial structures. If the distance of v is larger than a threshold, we add v as a new medial structure, otherwise, we stop the initialization. When the vertex v lies in a boundary, we also extend it to a loop. In our experiments, we set the threshold to $\kappa \overline{\mathcal{D}}$, where $\kappa \in [1,2]$ and $\overline{\mathcal{D}}$ is the average of the diffusion distance between the points in $\mathcal{R}$ and in $\mathcal{S}_{\mathcal{R}}$ (Eq. 15).

In the main loop, we refine the medial structures $\{\mathcal{S}_i\}$ iteratively, until achieving the bijection with the segments $\{\mathcal{R}_i\}$ (Fig. 2(c)). At each iteration, first we compete fronts from the medial structures to compose new segments. Then, we use these segments to update the medial structures. The above relaxation stops when the ratio of vertices in $\mathcal{R}$ changing segments is under a tolerance $(0-5\%)$.

To compete fronts, we create a heap H containing the pairs (f,i), where f is a candidate face to be covered by the front $\mathcal{F}_i$. The pairs are ordered in H by the maximum distance between the vertices of f and the medial structure $\mathcal{S}_i$,

$$\max_{v \in f} \left(\min_{u \in \mathcal{S}_i} \mathcal{D}^2_{t_{\mathcal{R}}}(v,u) \right). \tag{11}$$

We initialize H with all the faces adjacent to the vertices of the current medial structures $\{\mathcal{S}_i\}$. At each step, we remove the pair (f,i) with the smallest distance. If f is not in any segment, we add it to $\mathcal{R}_i$, otherwise, we discard it. After, we update H with the neighbor faces of f in $\mathcal{R}$. The competition ends when the heap is empty.

To update the medial structures, we compute the vertices with minimum *ADD* value in each segment $\mathcal{R}_i$ (Eq. 12). Because of the mesh resolution, the medial structures may be subsampled. We overcome these cases by adding a tolerance ε around the minimum *ADD* value. This tolerance must be close to zero and adapted to the shape of $\mathcal{R}_i$. In this work, we set $\varepsilon = 0.01\overline{ADD}$, where $\overline{ADD}$ is the average of the *ADD* values in $\mathcal{R}_i$ (Eq. 14).

We apply the above algorithm recursively, starting with $\mathcal{R} = \mathcal{M}$. The resulting segments compose a hierarchical tree. This hierarchy reveals a coarse-to-fine order of the segments, and a tree of dependencies. The final segmentation can be any cut of the tree (Fig. 4).
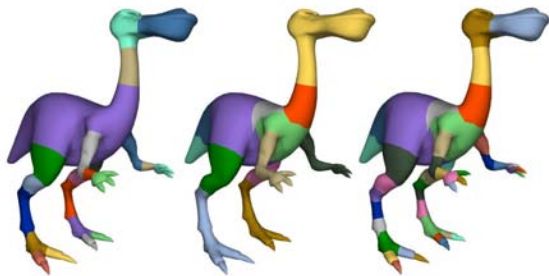

Figure 4: *Three different cuts of the hierarchy of segments of the* dinopet *model.*

4. Results

We tested our method with a diversity of models and poses. Fig. 5 shows a miscellaneous of results. In each example, we indicate the segments with a different palette of colors.

In Fig. 6, we show an example of the hierarchy of segments. Note that the segments enhance salient parts, as suggested by the cognition studies. The coarse segments correspond to functional regions (in green), and the fine segments correspond to rigid components (in yellow). The segments also reveal the structure of model, and enable the combination of different levels of details. In Fig. 4, we present three possible cuts of the hierarchy of segments of the *dinopet* model. In the first image, we partitioned the arms, the legs, and the head of the model, while, in the second image, we

divided only the core of the body. The third image shows a fine segmentation, identifying even the fingers of the hands and the nails of the toes.

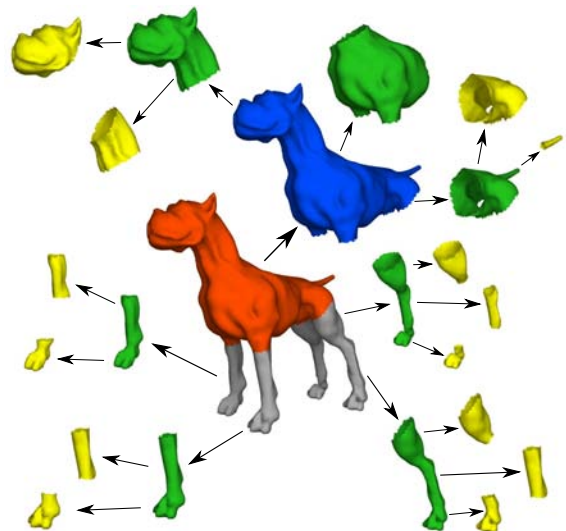**Figure 5:** *Results of our segmentation algorithm.*

Figure 6: *The hierarchical tree of segments of the* dog *model. Each color indicates a different level of detail.*

Fig. 9 illustrates the consistency of our results to a variety of deformations of three distinct models. In Fig. 1, we demonstrate that our segments are also consistent in successive scales. It is worth to note that our method resulted in consistent segments, even though each pose has a different mesh tessellation.

In Fig. 7, we show the robustness to noise of our algorithm. We perturbed the vertices of the *cat* model by moderate and exaggerated noise, and achieved segmentations similar to the segmentation of the original model. In

Fig. 8(a), we show that our method is robust to topological short-circuits, splitting the connected legs of the *homer* model. However, the method fails when the topological handle is large, as shown in Fig. 8(b). In this case, the handle alters the diffusion distance, and then the segmentation identifies only the remaining fingers of the hand.

Fig. 10 shows skeletons extracted from the segmentations. The skeletons are composed by edges connecting the centers of mass of the segments (blue spheres) to their adjacent articulations (gray spheres).

Table 1 reports running times. Notice that the number of iterations to converge the bijection between medial structures and segments is not larger than 10. Therefore, the time complexity of the algorithm depends on the cost of one iteration of the main loop, which is $O(|F|\log|F|)$, in the worst case. The most expensive step of our method is the computation of the eigen-pairs. Nonetheless, we compute them in a pre-processing phase and, using the solver proposed in [VL08], the cost reduces to the order of seconds.

Table 1: *Time report. The columns show, respectively, the name of the model, the numbers of vertices and faces, the time (sec.) to compute the eigen-pairs, the number of iterations, and the time (sec.) spent by our algorithm to compute the first level of detail. In all examples, we computed the first 200 eigen-pairs. The tests were performed on a 2.4GHz Intel Core 2 Duo with 2GB RAM.*

| model	$|V|$	$|F|$	solver	iters	level 1
dinopet	4k	8k	2.7	5	0.9
human	8k	16k	7.4	5	3.0
dog	9.5k	19k	9.2	6	4.7
armadillo	23k	46k	23.7	3	6.7
elephant	42k	84.5k	46.6	2	13.4
dinosaur	56k	112k	63.9	2	29.9

5. Conclusion and Future Work

In this paper, we presented a simple and fast algorithm to segment articulated characters. Our results compose a coarse-to-fine hierarchy of details, and reveal the underneath structure of the models. The method is invariant to deformations, even though the input is a single pose. In addition, we guarantee robustness to noise, mesh resolution, and topological short-circuits.

We described the algorithm for triangulated meshes, but it is straightforward to convert it to other surface representations. We also introduced a new definition of medial structures. Coupled with the segments, the medial structures can be employed in problems of model compression, registration, matching, and morphing.

In the future, we intend to continuously exploit the diffusion distance. We believe the diffusion distance can determine the skinning weights along the segments, complementing our method into a full rigging procedure. Finally, we would like to extend the scope of our segmentation for non-articulated models.

(a) Original   (b) Moderate   (c) Exaggerated
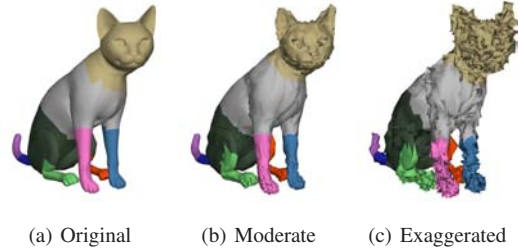
Figure 7: *Our method is robust to noise. The images compare the segmentations of the original model with two versions modified by moderate and exaggerated noise.*

(a)   (b)
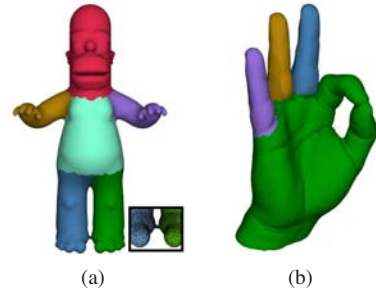
Figure 8: *(a) Our method is robust to short-topological events. (b) However, it fails with large handles.*

Appendix A:

In this last section, we provide the equations to compute the *ADD* value of a vertex, and the terms $\overline{ADD}$ and $\overline{\mathcal{D}}$ in a region $\mathcal{R}$ of a triangulated mesh $\mathcal{M} = (V, E, F)$ at time scale t.

Let A_f be the area of the triangle f, f_i be the i-th vertex of f, and $A_v = (\sum_{f \in star(v)} A_f)/3$ be the area in $\mathcal{R}$ of the vertex v. Here, $star(v)$ indicates the neighbor triangles in $\mathcal{R}$ of v.

The *ADD* function of a vertex (Eq. 7) is discretized as:

$$ADD(x) = \|\Phi_t(x)\|^2 - 2\left\langle \Phi_t(x), \frac{\int_{\mathcal{R}} \Phi_t(y)dy}{A_{\mathcal{R}}} \right\rangle + \frac{\int_{\mathcal{R}} \|\Phi_t(y)\|^2 dy}{A_{\mathcal{R}}}$$
$$\simeq \|\Phi_t(x)\|^2 - 2\left\langle \Phi_t(x), \frac{\sum_{v \in \mathcal{R}} \Phi_t(v)A_v}{A_{\mathcal{R}}} \right\rangle + Q_{\mathcal{R}}, \tag{12}$$

where

$$Q_{\mathcal{R}} = \frac{1}{6A_{\mathcal{R}}} \sum_{f \in \mathcal{R}} A_f \left(\sum_i \|\Phi_t(f_i)\|^2 + \langle \Phi_t(f_i), \Phi_t(f_{i+1 mod 3}) \rangle \right). \tag{13}$$

The average of the *ADD* function is:

$$\overline{ADD} = \frac{1}{A_{\mathcal{R}}} \int_{\mathcal{R}} ADD(x)dx \simeq 2\left(Q_{\mathcal{R}} - \left\| \frac{\sum_{v \in \mathcal{R}} \Phi_t(v)A_v}{A_{\mathcal{R}}} \right\|^2 \right). \tag{14}$$

At last, the average of the diffusion distances between the points of $\mathcal{R}$ and the points of the medial structure $\mathcal{S}_{\mathcal{R}}$ is:

$$
\begin{aligned}
\overline{\mathcal{D}} &= \tfrac{1}{A_{\mathcal{R}}} \int_{\mathcal{R}} \left(\min_{u \in \mathcal{S}_{\mathcal{R}}} \mathcal{D}_t^2(x,u) \right) dx \\
&\simeq \tfrac{1}{A_{\mathcal{R}}} \Big[\textstyle\sum_{v \in \mathcal{R}} \left(\min_{u \in \mathcal{S}_{\mathcal{R}}} \mathcal{D}_t^2(v,u) \right) A_v \\
&\quad + \textstyle\sum_{f \in \mathcal{R}} \tfrac{A_f}{6} \langle \Phi_t(f_3) - \Phi_t(f_1), \Phi_t(f_3) - \Phi_t(f_2) \rangle \\
&\quad - \textstyle\sum_{f \in \mathcal{R}} \tfrac{A_f}{6} \left(\|\Phi_t(f_3) - \Phi_t(f_1)\|^2 + \|\Phi_t(f_3) - \Phi_t(f_2)\|^2 \right) \Big] .
\end{aligned}
\tag{15}
$$

Note that the three equations can be computed with time complexity linear on the size of $\mathcal{R}$.
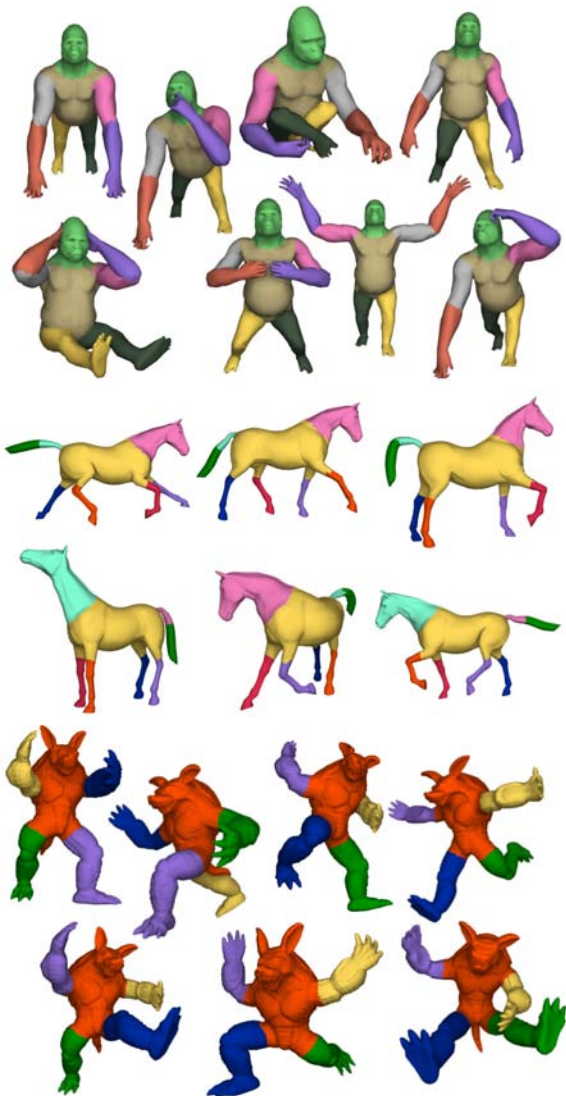
Figure 9: *A variety of poses for three distinct models, and the consistent segments generated with our method.*

References

[AKM*06] ATTENE M., KATZ S., MORTARA M., PATANE G., SPAGNUOLO M., TAL A.: Mesh segmentation - a comparative study. In *Proc. of the IEEE Intl. Conf. on Shape Modeling and Appl.* (2006), p. 7.

[AKP*04] ANGUELOV D., KOLLER D., PANG H.-C., SRINIVASAN P., THRUN S.: Recovering articulated object models from 3D range data. In *Proc. of the 20th conf. on uncertainty in artificial intelligence* (2004), pp. 18–26.

[Bas95] BASS R.: *Probabilistic Techniques in Analysis.* Springer-Verlag, 1995.

[CL06] COIFMAN R. R., LAFON S.: Diffusion maps. *Applied and Comp. Harmonic Analysis: Special issue on Diffusion Maps and Wavelets 21* (2006), 5–30.

[HR84] HOFFMAN D. D., RICHARDS W. A.: Parts of recognition. *Cognition 18* (1984), 65–96.

[HS97] HOFFMAN D. D., SIGNH M.: Salience of visual parts. *Cognition 63* (1997), 29–78.

[HSKK01] HILAGA M., SHINAGAWA Y., KOHMURA T., KUNII T. L.: Topology matching for fully automatic similarity estimation of 3d shapes. In *SIGGRAPH* (2001), ACM, pp. 203–212.

[JT05] JAMES D. L., TWIGG C. D.: Skinning mesh animations. In *SIGGRAPH* (2005), ACM, pp. 399–407.

[KJS07] KREAVOY V., JULIUS D., SHEFFER A.: Model composition from interchangeable components. In *15th Pacific Conf. on Comp. Graph. and Appl.* (2007), pp. 129–138.

[KLT05] KATZ S., LEIFMAN G., TAL A.: Mesh segmentation using feature point and core extraction. *The Visual Computer (Pacific Graph.) 21*, 8-10 (2005), 649–658.

[KS06] KRAYEVOY V., SHEFFER A.: Variational, meaningful shape decomposition. In *SIGGRAPH Technical Sketches* (2006), ACM, p. 50.

[KT03] KATZ S., TAL A.: Hierarchical mesh decomposition using fuzzy clustering and cuts. In *SIGGRAPH* (2003), ACM, pp. 954–961.

[LA04] LIEN J.-M., AMATO N. M.: Approximate convex decomposition of polyhedra. In *SIGGRAPH Posters* (2004), ACM, p. 2.

[LKA06] LIEN J.-M., KEYSER J., AMATO N. M.: Simultaneous shape decomposition and skeletonization. In *Proc. of the ACM Symp. on solid and physical modeling* (2006), pp. 219–228.

[LLS*05] LEE Y., LEE S., SHAMIR A., COHEN-OR D., SEIDEL H.-P.: Mesh scissoring with minima rule and part salience. *Comp. Aided Geom. Design 22*, 5 (2005), 444–465.

[LZ04] LIU R., ZHANG H.: Segmentation of 3D meshes through spectral clustering. In *12th Pacific Conf. on Computer Graphics and Appl.* (2004), pp. 298–305.
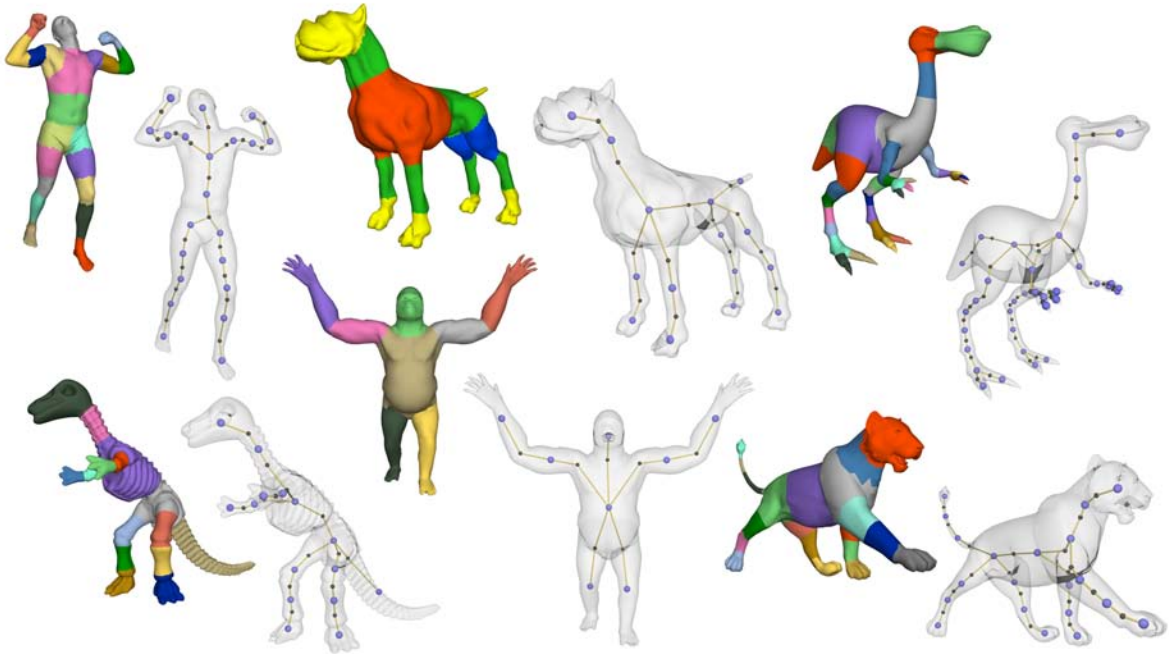
Figure 10: *Skeletons extracted from the segments. The blue spheres indicate the centers of mass of the segments, and the gray spheres indicate central points in the joints of the characters.*

[LZ07] LIU R., ZHANG H.: Mesh segmentation via spectral embedding and contour analysis. *Computer Graphics Forum (Special Issue of Eurographics) 26* (2007).

[MG03] MOHR A., GLEICHER M.: Building efficient, accurate character skins from examples. *ACM Trans. Graph. 22*, 3 (2003), 562–568.

[MPS*04] MORTARA M., PATANÈ G., SPAGNUOLO M., FALCIDIENO B., ROSSIGNAC J.: Plumber: a method for a multi-scale decomposition of 3D shapes into tubular primitives and bodies. In *Proc. of the ninth ACM symp. on solid modeling and applications* (2004), pp. 339–344.

[MW99] MANGAN A. P., WHITAKER R. T.: Partitioning 3D surface meshes using watershed segmentation. *IEEE Trans. on Vis. and Comp. Graphics 5*, 4 (1999), 308–321.

[PKA03] PAGE D. L., KOSCHAN A., ABIDI M.: Perception-based 3D triangle mesh segmentation using fast marching watersheds. In *Proc. of the Computer Vision and Pattern Recognition* (2003), pp. 27–32.

[Rus07] RUSTAMOV R. M.: Laplace-beltrami eigenfunctions for deformation invariant shape representation. In *Proc. of the fifth Eurographics Symp. on Geometry Processing (SGP)* (2007), pp. 225–233.

[RWP06] REUTER M., WOLTER F.-E., PEINECKE N.: Laplace-beltrami spectra as "shape-dna" of surfaces and solids. *Computer-Aided Design 38*, 4 (2006), 342–366.

[Sha04] SHAMIR A.: A formulation of boundary mesh segmentation. In *Proc. of the 2nd Intl. Symp. on 3D Data Proc., Visualization, and Transmission* (2004), pp. 82–89.

[Sha06] SHAMIR A.: Segmentation and shape extraction of 3D boundary meshes. In *State-of-art Report: Eurographics* (2006), pp. 137–149.

[SSCO08] SHAPIRA L., SHAMIR A., COHEN-OR D.: Consistent mesh partitioning and skeletonisation using the shape diameter function. *Visual Comp. 24*, 4 (2008), 249–259.

[STK02] SHLAFMAN S., TAL A., KATZ S.: Metamorphosis of polyhedral surfaces using decomposition. *Computer Graphics Forum 21*, 3 (2002), 219–228.

[SY07] SCHAEFER S., YUKSEL C.: Example-based skeleton extraction. In *Proc. of the fifth Eurographics Symp. on Geometry Processing* (2007), pp. 153–162.

[VL08] VALLET B., LEVY B.: Spectral geometry processing with manifold harmonics. *Computer Graphics Forum (Proc. Eurographics) 27*, 2 (2008).

[ZL05] ZHANG H., LIU R.: Mesh segmentation via recursive and visually salient spectral cuts. In *Proc. of Vision, Modeling, and Visualization* (2005), pp. 429–436.

[ZMT05] ZHANG E., MISCHAIKOW K., TURK G.: Feature-based surface parameterization and texture mapping. *ACM Trans. on Graph. 24*, 1 (2005), 1–27.